

Local paths to global coherence: cutting networks down to size

Yu Hu^{*1}, and James Trousdale^{*2}, Eric Shea-Brown^{†1,4}, and Krešimir Josić^{†2,3}

¹Department of Applied Mathematics, University of Washington, Seattle, WA 98195

²Department of Mathematics, University of Houston, Houston, TX 77204-5001

³Department of Biology and Biochemistry, University of Houston, Houston, TX 77204-5001

⁴Program in Neurobiology and Behavior, University of Washington, Seattle, WA 98195

June 25, 2022

Abstract

How does connectivity impact network dynamics? We address this question by providing a widely-applicable link between network characteristics on two scales. On the global scale we consider the coherence of overall network activity. We show that such global coherence can often be predicted from the local structure of the network. To characterize this local structure we introduce *motif cumulants*, which measure the deviation of pathway counts from those expected in a minimal probabilistic network model. Importantly, this link between global dynamics and local architecture is strongly affected by heterogeneity in the network connectivity. The relationship can be strengthened if the network is divided into connectivity-based subpopulations. Extensions of the theory relate higher-order (i.e., beyond pairwise) statistics of network-wide dynamics and more complex patterns of local connectivity.

^{*},[†] These authors contributed equally.

1 Introduction

From genetics to neuroscience to the social world, networks of stochastic dynamical systems are ubiquitous. The architecture of these networks is complex: irregular but far from random, with an overrepresentation of motifs and hubs [Bonifazi et al., 2009, Song et al., 2005, Perin et al., 2011, Milo et al., 2004, Larimer and Strowbridge, 2008]. At the same time, networks produce complex patterns of collective dynamics [Pecora and Carroll, 1998, Strogatz, 2000, Rinzel and Ermentrout, 1989]. The joint activity of pairs and groups of nodes is frequently quantified using correlations and cumulants [Renart et al., 2010, Pernice et al., 2011, 2012, Lindner et al., 2005, Schneidman et al., 2003]. These measures relate closely to information coding and propagation in networks [Averbeck et al., 2006, Salinas and Sejnowski, 2000]. But despite significant progress [Pernice et al., 2011, 2012, Renart et al., 2010, Ginzburg and Sompolinsky, 1994, Sejnowski, 1976], relating network activity and connectivity remains a challenge.

Here, our aim is to connect highly *local* features of a network’s connectivity – the frequency of small connection pathways, or motifs – with *global* measures of dynamical coherence. Our results hold for any stochastic network where node interactions can be described via linear response. These include linearized SDEs (Ornstein-Uhlenbeck) and shot noise processes [Gardiner, 2009] on networks; our findings for pairwise correlations also extend to integrate-and-fire neurons [Trousdale et al., 2012] and linearly interacting point processes (Hawkes models [Hawkes, 1971, Pernice et al., 2011]).

We generalize a framework introduced in [Hu et al., 2012, Pernice et al., 2011] to characterize network structure by the prevalence of certain pathways that connect subsets of nodes, quantified by what we call *motif moments* and *motif cumulants*. Motif moments give a normalized count of pathways of a given length (order). Motif cumulants describe deviations in pathway counts at each order from those in a minimal probabilistic model of network architecture. Intriguingly, we find that the widely-occurring models of *clustered networks* are highly complex by both measures: high order structure statistics contribute significantly to correlated activity. We discuss the origin of this complexity and demonstrate a method to resolve it. Finally, we show that the link between global network dynamics and local connectivity extends to higher order: n -th order correlations can be predicted from the statistics of pathways connecting n nodes.

Network models Many stochastic networks with linear interactions take the form

$$y_i(t) = x_i(t) + A_i * \sum_j \mathbf{W}_{ij} y_j(t). \quad (1)$$

The activity of the i^{th} node, $y_i(t)$, is determined by a (stochastic) baseline activity, $x_i(t)$, together with filtered network input. The weight matrix, \mathbf{W} , describes the connectivity. To focus on network architecture, we make several simplifications: (1) equal-strength connections, when present, *i.e.* $\mathbf{W} = w\mathbf{W}^0$ for an adjacency matrix \mathbf{W}^0 , (2) homogenous nodal dynamics, so that $A_i(t) = A(t)$, and (3) statistically uniform (across i) processes $x_i(t)$. These assumptions can be relaxed (cf. [Hu et al., 2012]).

Let $\mathbf{y}(t) = (y_1(t), \dots, y_N(t))^T$ and $\mathbf{x}(t) = (x_1(t), \dots, x_N(t))^T$, and write the Fourier transform of Eq. (1) in matrix form as¹

$$\tilde{\mathbf{y}}(\omega) = \tilde{\mathbf{x}}(\omega) + \tilde{A}(\omega)\mathbf{W}\tilde{\mathbf{y}}(\omega). \quad (2)$$

Here $\tilde{\mathbf{y}}(\omega) = \int \exp(-2\pi i\omega t)(\mathbf{y}(t) - \mathbf{E}[\mathbf{y}(t)])dt$, $\tilde{\mathbf{x}}(\omega)$ is defined similarly, and $\tilde{A}(\omega) = \mathcal{F}(A)(\omega) = \int_{-\infty}^{\infty} \exp(-2\pi i\omega t)A(t)dt$. If the spectral radius $\Psi(\tilde{A}(\omega)\mathbf{W}) < 1$, then Eq. (2), implies $\tilde{\mathbf{y}} = (\mathbf{I} - \tilde{A}\mathbf{W})^{-1}\tilde{\mathbf{x}}$, yielding the following relation between the matrices of cross-spectra:

$$\mathbf{S}_y(\omega) = (\mathbf{I} - \tilde{A}^*\mathbf{W})^{-1}\mathbf{S}_x(\omega)(\mathbf{I} - \tilde{A}\mathbf{W}^T)^{-1}. \quad (3)$$

Denote by \mathbf{a}^* complex conjugation without transposition. In Eq. (3), we used $\mathbf{S}_y(\omega) = \mathbf{E}[\tilde{\mathbf{y}}^*\tilde{\mathbf{y}}^T]$, $\mathbf{S}_x(\omega) = \mathbf{E}[\tilde{\mathbf{x}}^*\tilde{\mathbf{x}}^T]$, and the Wiener-Khinchin relation $\mathbf{S}_y(\omega) = \mathcal{F}(\mathbf{C}_y(\tau))$ between the cross-spectra and the covariance matrix $(\mathbf{C}_y(\tau))_{ij} = \mathbf{E}[(y_i(t) - \mathbf{E}[y_i(t)])(y_j(t + \tau) - \mathbf{E}[y_j(t + \tau)])]$. Note that under our homogeneity assumptions $\mathbf{S}_x(\omega) = S_x(\omega)\mathbf{I}$ is a scalar matrix.

As an illustration, consider Ornstein-Uhlenbeck (OU) processes, which have been used widely to model biological networks [Pedraza and van Oudenaarden, 2005, Tomioka et al., 2004, Lestas et al., 2008, Warren et al., 2005]. For such processes,

$$\dot{\mathbf{y}} = -\mathbf{\Lambda}\mathbf{y}(t) + \mathbf{W}\mathbf{y}(t) + \boldsymbol{\xi}(t), \quad (4)$$

where $\boldsymbol{\xi}(t)$ is a column vector of white noise processes (here assumed to be independent), $\mathbf{\Lambda} = \tau^{-1}\mathbf{I}$, and τ sets the intrinsic timescale of the nodes. Eqs. (2,3) hold *exactly* for the OU system, with $\tilde{A}(\omega) = (\tau^{-1} + 2\pi i\omega)^{-1}$ and $\tilde{\mathbf{x}}(\omega) = \tilde{A}(\omega)\boldsymbol{\xi}(\omega)$. An analog of Eq. (3) holds approximately in models of neuronal networks [Trousdale et al., 2012], and exactly for Hawkes processes [Hawkes, 1971]. Hence our findings about pairwise covariances extend to these systems.

Eq. (3) can be expanded in a series [Trousdale et al., 2012, Hu et al., 2012, Pernice et al., 2011],

$$\mathbf{S}_y(\omega)/S_x(\omega) = \sum_{n,m=0}^{\infty} \tilde{A}^{n*}\tilde{A}^m\mathbf{W}^n(\mathbf{W}^T)^m. \quad (5)$$

Here, we have normalized by $S_x(\omega)$ and the unitless quantity on the right measures network coherence (we can use this quantity to derive the approximate average correlation coefficient - see Supplementary Information (SI)).

Each term in the sum represents a contribution to the cross spectrum from a different path, or motif, in the network. Consider the second order term $\tilde{A}\tilde{A}^*(\mathbf{W}\mathbf{W}^T)_{ij} = w^2|\tilde{A}|^2 \sum_k \mathbf{W}_{ik}^0 \mathbf{W}_{jk}^0$. Here $w^2|\tilde{A}|^2 \mathbf{W}_{ik}^0 \mathbf{W}_{jk}^0$ gives the contribution to the spectrum of cells i and j of common input (if both connections are present) from node k . In general $(\mathbf{W}^n(\mathbf{W}^T)^m)_{ij}$ represents the contribution of (n, m) motifs - motifs consisting of two directed chains emanating from a single apex. Each chain terminates in nodes i and j after traversing n and m

¹Fourier transforms of stochastic processes should be interpreted as taken over finite windows of the processes: When computing spectral statistics, scale by $1/T$, and take the limit as $T \rightarrow \infty$. See [Laing and Lord, 2009].

nodes, respectively. A $(0, m)$ motif is a chain of length m from node i to node j . The same node can appear multiple times in a motif.

Fig. 1 illustrates this decomposition in a network of two mutually inhibiting nodes. The cross-covariance between the nodes, $(\mathbf{C}_y(\tau))_{12} = \mathcal{F}^{-1}(\mathbf{S}_y(\omega))_{12}$, is shown in Fig. 1(a), while contributions of low order motifs to $(\mathbf{C}_y(\tau))_{12}$ are given in Fig. 1(b). As motif order increases, corresponding contributions decrease in magnitude, but increase in width. The asymmetry of a contribution increases with the asymmetry of the associated motif, *i.e.* the difference between n and m in an (n, m) motif: Compare the contributions of the $(1, 2)$ and $(0, 3)$ motifs. A graphical decomposition of the circuit into the first few (n, m) motifs is shown in Fig. 1(c). Since the network is recurrent, the expansion in Eq. (5) does not terminate.

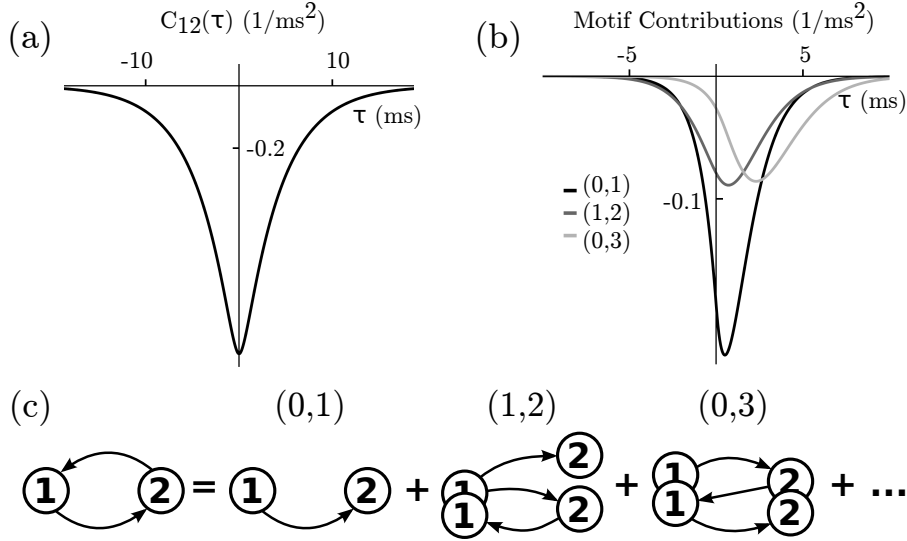


Figure 1: (a) The cross-correlation function of two mutually inhibiting nodes. (b) Contribution of first- and third-order motifs to the cross-correlation function in (a). (c) Graphical decomposition of the network showing motifs whose contributions are given in (b).

Cumulants, moments, and network-wide coherence We now show how averaged measures of network coherence depend on network structure. For concreteness – but without loss of generality [Trousdale et al., 2012] – we consider integrals of covariance functions over long time windows by evaluating all spectral quantities at $\omega = 0$. We indicate this by dropping the dependence on ω . Moreover, we compute network-wide averages of coherence. Denoting by $\langle \mathbf{X} \rangle$ the empirical average of the entries of matrix \mathbf{X} , we obtain from Eq. (5)

$$\begin{aligned}
 \langle \mathbf{S}_y \rangle / S_x &= \sum_{n,m=0}^{\infty} \tilde{A}^{n+m} \langle \mathbf{W}^n (\mathbf{W}^T)^m \rangle \\
 &=: \frac{1}{N} \sum_{n,m=0}^{\infty} (N \tilde{A} w)^{n+m} \boldsymbol{\mu}_{n,m}.
 \end{aligned} \tag{6}$$

Here the *motif moment*, $\boldsymbol{\mu}_{n,m} = \langle \mathbf{W}^{0n}(\mathbf{W}^{0T})^m \rangle / N^{n+m-1}$, is the empirical probability of observing an (n, m) motif in the network [Pernice et al., 2011, Hu et al., 2012]. Note that $\boldsymbol{\mu}_{n,m} = \boldsymbol{\mu}_{m,n}$. We define $\boldsymbol{\mu}_{n,0} = \boldsymbol{\mu}_n$, and let $\boldsymbol{\mu}_{0,0} = 1$.

Using Eq. (3), we follow [Hu et al., 2012] and obtain an alternate expansion in terms of *motif cumulants* [Hu et al., 2012]:

$$\frac{\langle \mathbf{S}_y \rangle}{S_x} = \frac{1}{N} \frac{\left(1 + \sum_{n,m=1}^{\infty} (N\tilde{A}w)^{n+m} \boldsymbol{\kappa}_{n,m}\right)}{\left(1 - \sum_{n=1}^{\infty} (N\tilde{A}w)^n \boldsymbol{\kappa}_n\right)^2}. \quad (7)$$

The relation between the motif cumulants, $\boldsymbol{\kappa}_{n,m}$, of Eq. (7) and the moments $\boldsymbol{\mu}_{n,m}$ is similar that between cumulants and moments of a random variable. Let $\mathcal{C}(n) = \left\{ \{n_1, \dots, n_t\} : \sum_i n_i = n \right\}$ be the set of all compositions (*ordered partitions*) of n . Then

$$\boldsymbol{\mu}_n = \sum_{\{n_1, \dots, n_t\} \in \mathcal{C}(n)} \left(\prod_{i=1}^t \boldsymbol{\kappa}_{n_i} \right) \quad (8)$$

$$\boldsymbol{\mu}_{n,m} = \sum_{\substack{\{n_1, \dots, n_t\} \in \mathcal{C}(n) \\ \{m_1, \dots, m_s\} \in \mathcal{C}(m)}} \left(\prod_{i=1}^{t-1} \boldsymbol{\kappa}_{n_i} \right) (\boldsymbol{\kappa}_{n_t, m_s} + \boldsymbol{\kappa}_{n_t} \boldsymbol{\kappa}_{m_s}) \left(\prod_{j=1}^{s-1} \boldsymbol{\kappa}_{m_j} \right) \quad (9)$$

In evaluating these terms, we take $\left(\prod_{i=1}^{t-1} \boldsymbol{\kappa}_{n_i}\right) = 1$ if $t = 1$ and likewise if $s = 1$.

The construction of motif moments from cumulants has a familiar interpretation: estimating the probability of a joint event from the probability of its constituents. Fig. 2(a) demonstrates this for two example motifs. Each term in the diagrammatic expansion arises from a cumulant. The first order term gives the probability assuming independence of each connection, and the subsequent terms give corrections from excess occurrences of second, and then higher-order, submotifs. Hence, each motif cumulants, $\boldsymbol{\kappa}_{n,m}$ captures “pure” higher order connectivity statistics. For an explicit expression for the motif cumulants $\boldsymbol{\kappa}_{n,m}$, see the SI and [Hu et al., 2012].

As an illustrative example, we consider a special case of the two-cluster *stochastic block model* [Wang and Wong, 1987, Daudin et al., 2008, Litwin-Kumar and Doiron, 2012]. Such networks are comprised of two subpopulations, each of size $N/2$, and associated with a constant s_i . The connection probability between nodes in subpopulation i and j is $p_{ij} = s_i s_j$, and hence $p_{ii} = s_i^2$ within subpopulation i . While fixing the overall connection probability p , the difference between s_1 and s_2 describes the degree of clustering in the network. When $s_2 = 0$ ($s_1 = 2\sqrt{p}$), the only connections are between nodes in the first subpopulation. The case $s_1 = s_2 = \sqrt{p}$ corresponds to an Erdős-Rényi (ER) network.

Expansions (6) and (7) deliver complementary information about the role of network paths in generating coherent activity. Truncating Eq. (6) at order k_{\max} , so that $n+m \leq k_{\max}$, gives the covariance due to paths up to length k_{\max} . A similar truncation of Eq. (7) gives the covariance of paths of all orders, with frequencies *predicted* from paths up to order k_{\max} .

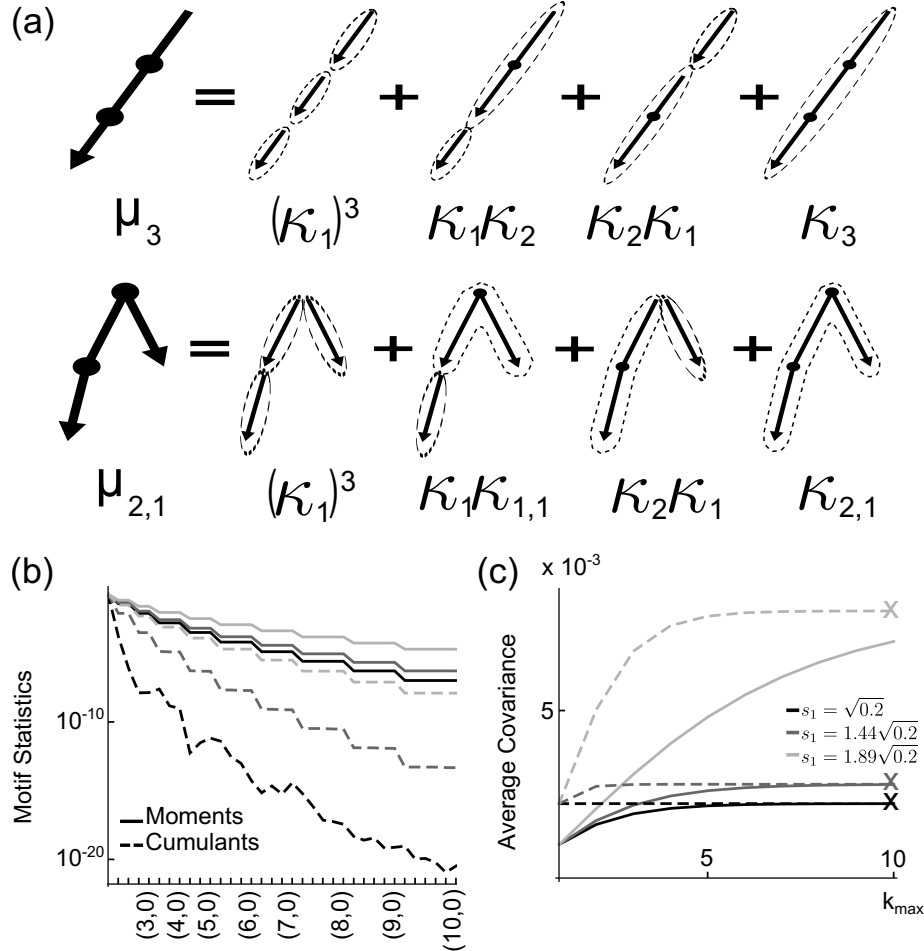


Figure 2: (a) The probability of observing two example motifs decomposed into *motif cumulants* of the graph. (b) The magnitude of motif cumulants (dashed lines) and moments (solid lines) for stochastic block networks: (n, m) motifs with $n \geq m$ were grouped first by $n + m$ and then arranged by increasing n . (c) Approximations of average covariances using motif moments (Eq. (6), solid lines) and cumulants (Eq. (7), dashed lines) up to order k_{\max} . Exact values (direct evaluation of Eq. (3)) are labeled by crosses. Throughout, we use stochastic block models of size 1000 and connection probability 0.2 but with different degree of clustering (lighter shades are more clustered).

Fig. 2(b) shows that motif cumulants decay more rapidly than motif moments. Thus, predictions of correlations based on cumulants rather than motifs will be more accurate at a given order. Second, both motifs and cumulant terms of orders > 1 are larger for more heterogeneous networks. This suggests that heterogeneity in a network’s architecture introduces a dependence of correlations on longer paths and more complex network structures.

Fig. 2(c) illustrates that the difference is important. At any given order cumulants yield more accurate estimates of network coherence. Intriguingly, higher order motif cumulants are needed to capture average covariance for other heterogeneous networks. We found that networks generated using the Barabasi-Albert (BA) model behaves similarly to a highly clustered network [Prettejohn et al., 2011] (see SI), a point we return to below.

These results agree with our intuition about when local connectivity is a good predictor of global dynamics. ER networks are homogeneous, and the most local network statistic – connection probability – fully determines graph structure. Thus, for nearly ER networks, low order motif cumulants predict dynamical coherence. On the other hand, highly clustered networks feature heterogeneous probabilities of linking different nodes. As a consequence, the frequency of large motifs depends jointly on multiple connectivity statistics, and cannot be obtained accurately from frequencies of lower order motifs exclusively. We next identify a novel way of grouping nodes to tame these effects and reestablish the link between local connectivity and global coherence.

Subpopulation cumulants Subsets of nodes can be grouped into classes, or subpopulations, that share features of dynamics or connectivity. We focus on the latter possibility, and characterize each subpopulation by its own motif statistics. Specifically, for b subpopulations, $\boldsymbol{\mu}_{n,m}$ becomes a $b \times b$ matrix of moments. Entry p, q is the empirical probability of an (n, m) motif with end nodes belonging to populations p and q , respectively. Motif cumulants $\boldsymbol{\kappa}_{n,m}$ are defined by a recursive relationships similar to Eqs. (8,9), with products interpreted as matrix multiplications (See SI Eqs. (25, 26)).

We can extend Eq. (7) to approximate average covariances using motif statistics within and across subpopulations (Eq. (15) in the SI). Fig. 3(a) illustrates this approach using the stochastic block model. If the two sets of nodes used in the generation of the graph define the two subpopulations, first order motif cumulants alone predict average correlations perfectly (compare with Fig. 2(b)).

Importantly, the subpopulation approach also works when there is no obvious grouping of nodes. As an example we consider finite networks obtained using the BA model. These are highly heterogeneous networks with power law degree distributions. If we order the nodes according to the sum of in- and out-degree, two subpopulations can be formed from nodes with degrees above and below a given threshold value. Fig. 3(b) shows that resulting predictions of network correlations are significantly improved if the threshold is chosen properly.

With an increasing number of subpopulations, b , we expect the accuracy of predicted correlations to increase. As b increases, so does the number of subpopulation statistics at our disposal. Thus we have a tradeoff between the resolution in motif statistics at each order

and the minimal motif size needed to achieve a given accuracy. As expected, more detailed information about local connectivity leads to a better description of global coherence.

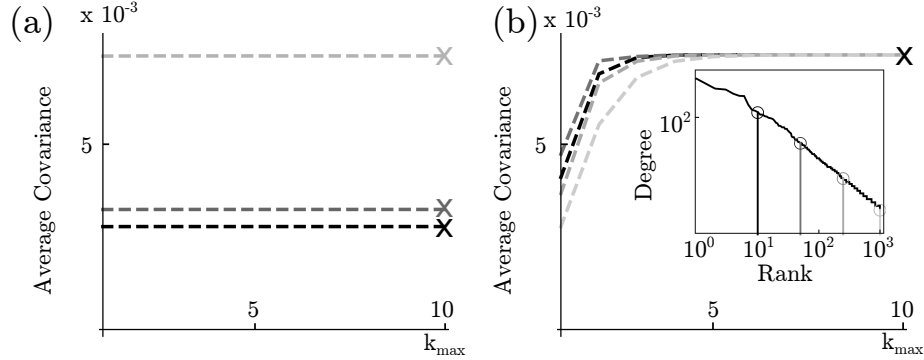


Figure 3: Approximations of average covariances using the subpopulation cumulant approach and truncating at order k_{\max} . Exact values obtained by evaluating Eq. (3) are labeled by crosses. (a) stochastic block model networks of Fig. 2 (the colors are the same) divided into two subpopulations with differing connectivities; (b) BA network divided into two subpopulations according to different thresholds on the sum of in- and out-degrees (different colors, see inset).

Higher order correlations We can similarly relate higher order statistics of a network’s dynamics to its architecture. Our results apply to continuous-valued processes; extensions to higher-order coherence for *interacting point processes* are nontrivial and will be tackled in future work. Consider again stationary stochastic processes $\mathbf{y}(t) = (y_1(t), \dots, y_N(t))^T$. The k^{th} order cross-covariance function is defined using joint cumulants of random variables,

$$C_{y[k]}^{i_1 i_2 \dots i_k}(\tau_1, \dots, \tau_{k-1}) := \kappa(y_{i_1}(t), y_{i_2}(t + \tau_1), \dots, y_{i_k}(t + \tau_{k-1})). \quad (10)$$

A generalization of the Wiener-Khinchin theorem relates the Fourier transform of the higher order cumulant to the polyspectra $\mathbf{S}_y^{i_1 i_2 \dots i_k}$ defined via the Fourier transform of the processes [Brillinger, 1964]. At third order, we have the bispectrum $\mathcal{F}(C_{y[3]}^{i_1 i_2 i_3}(\tau_1, \tau_2)) = \mathbf{S}_{y[3]}^{i_1 i_2 i_3}(\omega_1, \omega_2) := \mathbf{E}[\tilde{y}_{i_1}^*(\omega_1 + \omega_2)\tilde{y}_{i_2}(\omega_1)\tilde{y}_{i_3}(\omega_2)]$. Using Eq. (2),² we can generalize Eq. (3) to obtain the bispectrum for the processes $\tilde{\mathbf{y}}$ in terms of that for $\tilde{\mathbf{x}}$ and the transfer matrix $\tilde{\mathbf{P}} = (\mathbf{I} - \tilde{\mathbf{A}}\mathbf{W})^{-1}$:

$$\mathbf{S}_{y[3]}^{i_1 i_2 i_3}(\omega_1, \omega_2) = \sum_{j_1, j_2, j_3} \tilde{\mathbf{P}}_{i_1 j_1}^*(\omega_1 + \omega_2) \tilde{\mathbf{P}}_{i_2 j_2}(\omega_1) \tilde{\mathbf{P}}_{i_3 j_3}(\omega_2) \mathbf{S}_{x[3]}^{j_1 j_2 j_3}(\omega_1, \omega_2). \quad (11)$$

Expanding $\mathbf{P} = \sum_{n=0}^{\infty} (\tilde{\mathbf{A}}\mathbf{W})^n$ in Eq. (11) leads to an expression for third order polyspectra analogous to Eq. (5):

$$\langle \mathbf{S}_{y[3]} \rangle / S_{x[3]} = \frac{1}{N^2} \sum_{n, m, l=0}^{\infty} (N\tilde{\mathbf{A}}\mathbf{w})^{n+m+l} \boldsymbol{\mu}_{n, m, l} \quad (12)$$

²Replacing Gaussian white noise in the OU process with “Poisson kicks”, *i.e.* considering a shot noise process, yields non-zero $\mathbf{S}_{x[3]}$

(for simplicity, we again set $\omega_1 = \omega_2 = 0$). Assuming homogeneity, the bispectrum for the uncoupled network $\mathbf{S}_{x[3]} = S_{x[3]} \mathbf{I}_{x[3]}$ is a diagonal tensor. More general structure, as well as common input, can be treated similarly [Hu et al., 2012]. Here, the motif moments describe contributions of 3-branch motifs (Fig. 4): $\mu_{n,m,l} = N^{-(n+m+l+1)} \sum_{i,j,k,o=1}^N (\mathbf{W}^{0n})_{io} (\mathbf{W}^{0m})_{jo} (\mathbf{W}^{0l})_{ko}$.

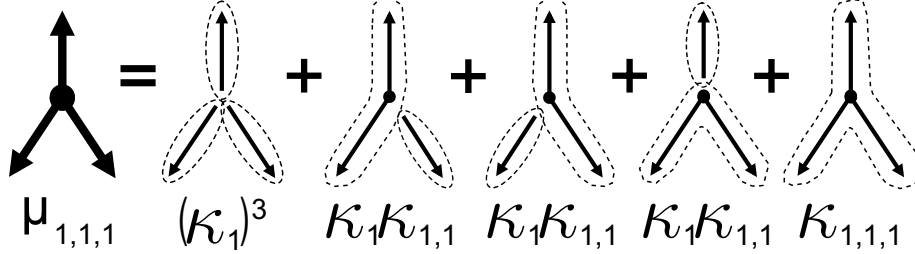


Figure 4: Cumulant decomposition of a three-branch motif.

A generalization of Prop. 4.1 in [Hu et al., 2012], allows us to extend Eq. (7) to predict network-wide third order correlations in terms of motif cumulants:

$$\frac{\langle \mathbf{S}_{y[3]} \rangle}{S_{x[3]}} = \frac{1}{N^2} \left(1 - \sum_{n=1}^{\infty} (N \tilde{A} w)^n \kappa_n \right)^{-3} \cdot \left(1 + 3 \sum_{l,m=1}^{\infty} (N \tilde{A} w)^{l+m} \kappa_{l,m} + \sum_{l,m,n=1}^{\infty} (N \tilde{A} w)^{l+m+n} \kappa_{l,m,n} \right). \quad (13)$$

Here we use three branch motif cumulants $\kappa_{n,m,l}$ which have a similar graphical interpretation to their second order counterparts (Fig. 4). The third order motif cumulants may again be recursively defined in terms of the motif moments:

$$\mu_{n,m,l} = \sum_{\substack{\{n_1, \dots, n_t\} \in \mathcal{C}(n) \\ \{m_1, \dots, m_s\} \in \mathcal{C}(m) \\ \{l_1, \dots, l_r\} \in \mathcal{C}(l)}} \left(\prod_{i=1}^{t-1} \kappa_{n_i} \right) \left(\prod_{j=1}^{s-1} \kappa_{m_j} \right) \left(\prod_{k=1}^{r-1} \kappa_{l_k} \right) \cdot (\kappa_{n_t, m_s, l_r} + \kappa_{n_t, m_s} \kappa_{l_r} + \kappa_{m_s, l_r} \kappa_{n_t} + \kappa_{n_t, l_r} \kappa_{m_s} + \kappa_{n_t} \kappa_{m_s} \kappa_{l_r}) \quad (14)$$

with the sum being over compositions of n, m, l defined as in Eqs. (8,9).

Our observations for second order statistics generalize directly: Higher order statistics of local connectivity predict higher order statistics of network wide dynamics (see SI Fig. 6). First, for both stochastic block models and the BA network, correlations depend significantly on long interaction paths through the networks, and on higher-order motifs. Second, at a given motif order, motif cumulants provide more accurate predictions of correlations. Third, the order of motif statistics needed to approximate correlations again increases with network heterogeneity. Finally, the subpopulation approach also generalizes to third order and offers similar advantages in predicting correlations from lower-order motif cumulants (see SI Fig. 7).

Conclusion: For a class of networks with dynamics described by linear response – perhaps around an operating point determined by the fully nonlinear dynamics – we have quantified the link between local network connectivity and global coherence in activity. In identifying the key quantities – motif cumulants – we provide a tool to identify what connection features matter most, and least, in determining collective network dynamics. Moreover, these cumulants are both efficient and flexible, in terms of their definition and their ability to predict activity based on connection data from small subgroups of nodes. This property could provide a way forward in experimental settings – as in studies of networks of genes [Alon, 2007] or neurons [Song et al., 2005, Perin et al., 2011] – in which networks are quantified by a limited number of edges are measured simultaneously.

Acknowledgements

We thank C. Hoffman, K. Bassler and B. Doiron for helpful insights and suggestions. This work was supported by NSF grants DMS-0817649, DMS-1122094, a Texas ARP/ATP award to KJ, and by a Career Award at the Scientific Interface from the Burroughs Wellcome Fund and NSF Grants DMS-1056125 and DMS-0818153 to ESB.

References

- U. Alon. Network motifs: theory and experimental approaches. *Nature Reviews Genetics*, 8(6):450–461, 2007.
- B. B Averbeck, P. E. Latham, and A. Pouget. Neural correlations, population coding and computation. *Nat Rev Neurosci*, 7:358–366, 2006.
- P Bonifazi, M Goldin, M A Picardo, I Jorquera, A Cattani, G Bianconi, A Represa, Y Ben-Ari, and R Cossart. The neuroscientist comments. *Science (New York, NY)*, 326(5958):1419–24, Dec 2009. doi: 10.1126/science.1175509.
- David R Brillinger. An introduction to polyspectra, 1964.
- F. Chung and L. Lu. Connected components in random graphs with given expected degree sequences. *Annals of combinatorics*, 6(2):125–145, 2002.
- J.J. Daudin, F. Picard, and S. Robin. A mixture model for random graphs. *Statistics and computing*, 18(2):173–183, 2008.
- CW Gardiner. *Handbook of Stochastic Methods for Physics, Chemistry and the Natural Sciences*. Springer-Verlag, Berlin, 2009.
- I. Ginzburg and H. Sompolinsky. Theory of correlations in stochastic neural networks. *Physical Review E*, 50(4):3171, 1994.

- A.G. Hawkes. Point spectra of some mutually exciting point processes. *J Roy Stat Soc B Met*, 33(3):438–443, 1971.
- Yu Hu, James Trousdale, Krešimir Josić, and Eric Shea-Brown. Motif Statistics and Spike Correlations in Neuronal Networks. *arXiv.org*, q-bio.NC, June 2012.
- Carlo Laing and Gabriel J Lord. *Stochastic Methods in Neuroscience*. Oxford University Press, September 2009.
- P. Larimer and B.W. Strowbridge. Nonrandom local circuits in the dentate gyrus. *The Journal of Neuroscience*, 28(47):12212–12223, 2008.
- Ioannis Lestas, Johan Paulsson, Nicholas E Ross, and Glenn Vinnicombe. Noise in Gene Regulatory Networks. *IEEE Transactions on Automatic Control*, 53(Special Issue):189–200, 2008.
- B. Lindner, B. Doiron, and A. Longtin. Theory of oscillatory firing induced by spatially correlated noise and delayed inhibitory feedback. *Phys Rev E*, 72(6):061919, 2005.
- A Litwin-Kumar and B Doiron. Slow dynamics and high variability in balanced cortical networks with clustered connections. *Nature Neuroscience*, 2012.
- Ron Milo, Shalev Itzkovitz, Nadav Kashtan, Reuven Levitt, Shai Shen-Orr, Inbal Ayzenshtat, Michal Sheffer, and Uri Alon. Superfamilies of evolved and designed networks. *Science (New York, NY)*, 303(5663):1538–1542, March 2004.
- Louis Pecora and Thomas Carroll. Master Stability Functions for Synchronized Coupled Cell Systems. *Phys. Rev. Lett.*, 80(10):2109, February 1998.
- Juan M Pedraza and Alexander van Oudenaarden. Noise propagation in gene networks. *Science (New York, NY)*, 307(5717):1965–9, Mar 2005. doi: 10.1126/science.1109090.
- R. Perin, T.K. Berger, and H. Markram. A synaptic organizing principle for cortical neuronal groups. *P Natl Acad Sci USA*, 108(13):5419–5424, 2011.
- V. Pernice, B. Staude, S. Cardanobile, and S. Rotter. Recurrent interactions in spiking networks with arbitrary topology. *Phys Rev E*, 85(031916), Mar 2012.
- Volker Pernice, Benjamin Staude, Stefano Cardanobile, and Stefan Rotter. How structure determines correlations in neuronal networks. *PLoS Comput Biol*, 7(5):e1002059, 05 2011. doi: 10.1371/journal.pcbi.1002059.
- B.J. Pettejohn, M.J. Berryman, and M.D. McDonnell. Methods for generating complex networks with selected structural properties for simulations: a review and tutorial for neuroscientists. *Frontiers in Computational Neuroscience*, 5, 2011.
- A. Renart, J. de la Rocha, P. Bartho, L. Hollender, N. Parga, A. Reyes, and K.D. Harris. The asynchronous state in cortical circuits. *Science*, 327(5965):587–590, 2010.

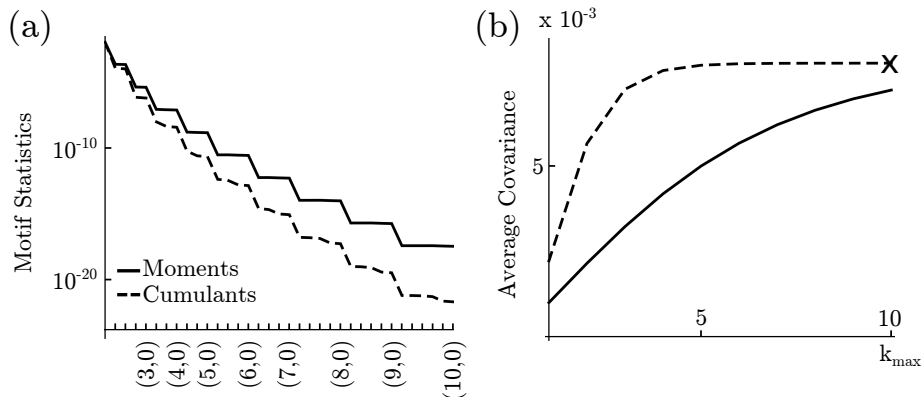
- J. Rinzel and G.B. Ermentrout. Analysis of neural excitability and oscillations. In C. Koch and I. Segev, editors, *Methods in neuronal modeling*, pages 135–169. MIT Press, 1989.
- E. Salinas and T. J. Sejnowski. Impact of correlated synaptic input on output firing rate and variability in simple neuronal models. *J Neurosci*, 20:6193–6209, 2000.
- Elad Schneidman, Susanne Still, Michael J Berry, and William Bialek. Network Information and Connected Correlations. *Physical Review Letters*, 91(23):238701, December 2003.
- T. Sejnowski. On the stochastic dynamics of neuronal interaction. *Biological Cybernetics*, 22:203–211, 1976.
- S. Song, P.J. Sjöström, M. Reigl, S. Nelson, and D.B. Chklovskii. Highly nonrandom features of synaptic connectivity in local cortical circuits. *PLoS Biol*, 3(3):e68, 2005.
- S. Strogatz. From Kuramoto to Crawford: Exploring the onset of synchronization in populations of coupled oscillators. *Physica D*, 143:1–20, 2000.
- Ryota Tomioka, Hidenori Kimura, Tetsuya J Kobayashi, and Kazuyuki Aihara. Multivariate analysis of noise in genetic regulatory networks. *Journal of Theoretical Biology*, 229(4):501–521, August 2004.
- James Trousdale, Yu Hu, Eric Shea-Brown, and Krešimir Josić. Impact of network structure and cellular response on spike time correlations. *PLoS Comput Biol*, 8(3):e1002408, 2012.
- Y J Wang and G Y Wong. Stochastic blockmodels for directed graphs. *Journal of the American Statistical Association*, 82(397):8–19, 1987.
- P B Warren, S Tanase-Nicola, and P R Wolde. Exact results for noise power spectra in linear biochemical reaction networks. *arXiv preprint q-bio/0512041*, 2005.

Supplementary Information for *Local paths to global coherence: cutting networks down to size*

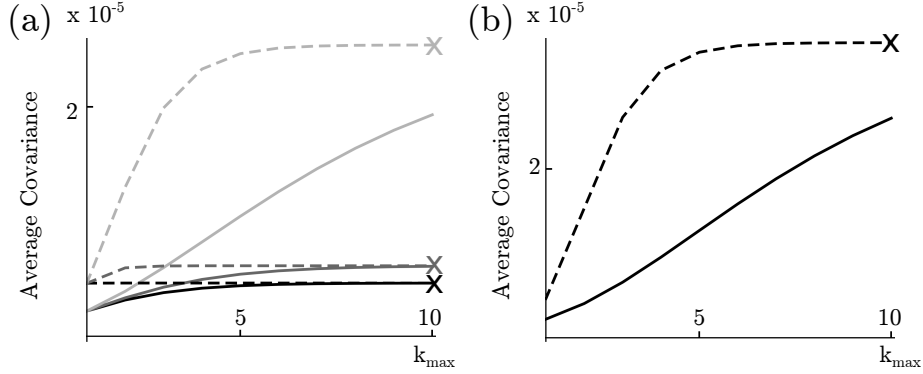
Further examples

Here we provide details of several computational findings referred to in the main text. Each addresses the generality and applicability of our results. First, SI Fig. 5 shows that our main results contrasting motif moments and cumulants hold for the Barábasi-Albert network model, which has significantly more complex structure than the stochastic block models studied in Fig. 2 of the main text.

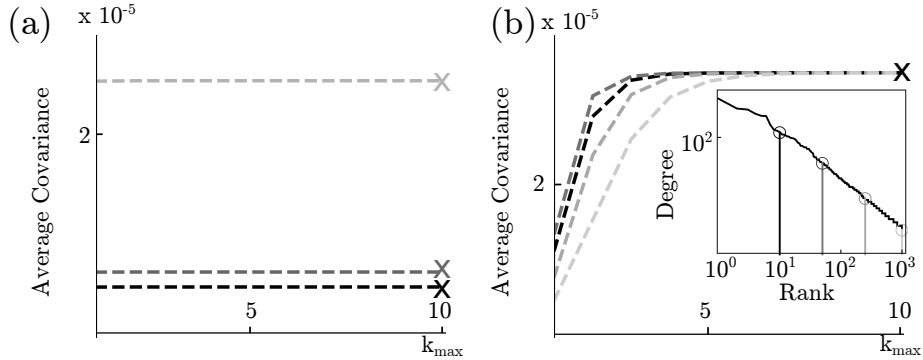
Next, SI Figs. 6 and 7 present analogous results for third-order correlations in network output. Specifically, SI Fig. 6 shows that these third-order correlations depend significantly on the details of the underlying graph structure (i.e., the degree of clustering). Moreover, this dependence can be efficiently predicted via motif cumulants. SI Fig. 7 demonstrates that the subpopulation approaches continue to enhance the accuracy of our predictions – if the populations are correctly defined, levels of triplet correlations can be predicted from lower-order motifs.



SI Fig. 5: Same as Fig. 2(b,c) of the main text but for the Barábasi-Albert model. (a) The magnitude of motif cumulants (dashed lines) and moments (solid lines) for a Barábasi-Albert model network. Motifs (n, m) , $n \geq m$ are grouped first by $n + m$ and then arranged by increasing n . (b) Approximations of average covariances using motif moments (truncating Eq. (6), solid lines) and cumulants (truncating Eq. (7), dashed lines) up to order k_{\max} . Exact values (direct evaluation of Eq. (3)) are labeled by crosses: a Barábasi-Albert network of size 1000 and connection probability 0.01.



SI Fig. 6: Same plots as Fig. 2(b) of the main text and SI Fig. 5(b) but for average third order correlations $\langle \mathbf{S}_{y[3]} \rangle / S_{x[3]}$. (a) Approximations using motif moments (truncating Eq. (12) of the main text, solid lines) and cumulants (truncating Eq. (13) of the main text, dashed lines) up to order k_{\max} . Exact values (direct evaluation of Eq. (11) of the main text) are labeled by crosses. Graphs were generated from stochastic block models of size 1000 and connection probability 0.2 but with different degree of clustering (lighter shades are more clustered). (b) Approximations using motif moments (solid lines) and cumulants (dashed lines) up to order k_{\max} for a Barabasi-Albert network of size 1000 and connection probability 0.01.



SI Fig. 7: Same plots as Fig. 3 of the main text but for average third order correlations $\langle \mathbf{S}_{y[3]} \rangle / S_{x[3]}$. Approximations using the subpopulation cumulant approach by truncating at order k_{\max} , the exact values (direct evaluation of Eq. (11) of the main text) are labeled by crosses: (a) stochastic block model networks of Fig. 2 of the main text (the colors are the same) divided into two subpopulations with differing connectivities; (b) the Barabasi-Albert network of SI Fig. 5 divided into two subpopulations according to different thresholds on the sum of in- and out-degrees (different colors, see also the inset, which displays the cutoffs).

Details of numerical results

Here we provide a detailed description of the computational examples provided in the main text and Supplementary Information. This includes all parameters describing the dynamics of nodes and connections, and our methods of generating random networks.

In Fig. 1 of the main text, we calculated correlations for an OU system (see Eq. (4) of the main text) with $\tau = 1$, $\boldsymbol{\xi}$ having unit intensity, and

$$\mathbf{W} = \begin{bmatrix} 0 & -0.75 \\ -0.75 & 0 \end{bmatrix}.$$

In plots of approximations of average second and third order covariances, i.e. Fig. 2(b), 3(a,b) of the main text, SI Figs. 5(b), 6(a,b), 7(a,b) and 8(b), the parameters \tilde{A} and w are chosen so that $N\tilde{A}wp = 0.4$. Note that the choice of S_x (resp. $S_{x[3]}$ at third order) will not affect the normalized quantity $\langle \mathbf{S}_y \rangle / S_x$ (resp. $\langle \mathbf{S}_{y[3]} \rangle / S_{x[3]}$), and can be set to 1.

The Barábasi-Albert networks in Fig. 3(b), and SI Figs. 5(a,b), 6(b), 7(b) and 8(b) are generated by a directed Barábasi-Albert model similar to that in [Prettejohn et al., 2011]. One starts with a “core” of Np nodes, randomly connected with connection probability 0.5. After that, $N - Np$ nodes are added to the graph. When adding a new node $i + 1$, it will form exactly Np connections with the existing nodes $1, \dots, i$. Those connections are distributed among existing nodes according to probabilities that are proportional to the sum of in- and out- degree of each node. The direction of the connection, whether into node $i + 1$ or out of node $i + 1$, is chosen independently with probability 0.5. The code implementing this algorithm is available upon request.

Explaining the effectiveness of the subpopulation motif approach

Mathematical underpinnings: In [Hu et al., 2012], we offered an intuition of the improvement in the rate of convergence of the motif cumulant approach (Eq. (7)) over the motif moment approach (Eq. (6)). Using the definitions $\mathbf{u} = (1, \dots, 1)^T / \sqrt{N}$, $\mathbf{H} = \mathbf{u}\mathbf{u}^T$, $\boldsymbol{\Theta} = \mathbf{I} - \mathbf{H}$, we compared the spectrum of \mathbf{W}^0 and $\mathbf{W}^0\boldsymbol{\Theta}$, which are related to the decay speed of $\boldsymbol{\mu}_{n,m}$ and $\boldsymbol{\kappa}_{n,m}$ respectively. $\mathbf{W}^0\boldsymbol{\Theta}$ usually has a much smaller spectral radius since $\mathbf{W}^0\boldsymbol{\Theta}$ essentially removed the largest isolated eigenvalue λ_{\max} . This can be seen from $\mathbf{W}^0\boldsymbol{\Theta}\mathbf{e} = 0$, where $\mathbf{e} = (1, \dots, 1)^T$ is close to the eigenvector associated with the largest eigenvalue in a “homogeneous” network (for example Erdős-Rényi network).

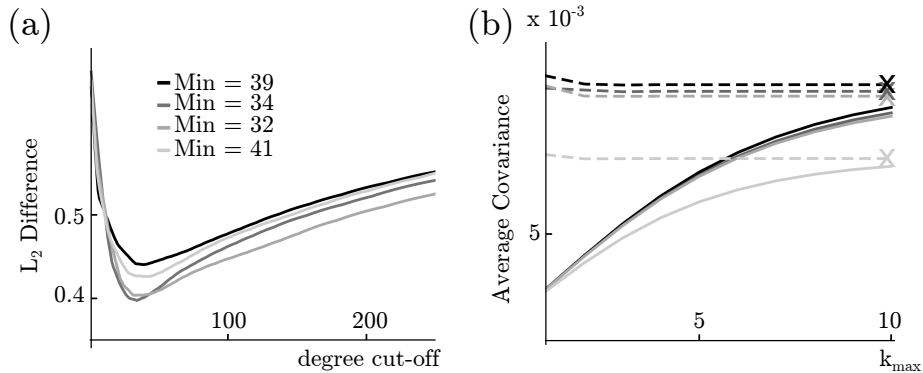
This reasoning can be extended to treat heterogeneous networks, such as the Barábasi-Albert network and stochastic block networks considered here. We begin with the observation that the eigenvector for λ_{\max} is approximately the (in) degree list \mathbf{d} (in our Barábasi-Albert networks, the in- and out- degrees are highly correlated). This is also the case for stochastic block models. In fact, for any adjacency matrix approximately having the form $\mathbf{W} = \mathbf{a}\mathbf{b}^T$ (\mathbf{a}, \mathbf{b} are column vectors), \mathbf{a} is the right eigenvector with eigenvalue $\mathbf{b}^T\mathbf{a}$. This indicates that the ideas that follow should hold for a general class of networks, including for the Chung and Lu model [Chung and Lu, 2002].

We next apply this to subpopulation motifs for heterogeneous networks. Using the same definition of $\boldsymbol{\Theta}$ as two paragraphs above will not work in eliminating the remapping largest eigenvalue of \mathbf{W}^0 to 0. This is because $\mathbf{W}^0\boldsymbol{\Theta}\mathbf{d}$ will not be close to 0, since $\boldsymbol{\Theta}$ maps only constant vectors to 0. The key in the subpopulation approach is to first redefine the $\boldsymbol{\Theta}$ matrix with a block diagonal structure, as detailed below SI Eq. (27). Such a $\boldsymbol{\Theta}$ will map

any vector that is piecewise constant over the indices of each subpopulation to 0. As a result, for stochastic block models $\mathbf{W}^0\Theta\mathbf{d} = 0$, exactly when using the natural division into subpopulations.

For the Barábasi-Albert network, this can only be achieved approximately using only two subpopulations and corresponding block diagonal Θ . A heuristic argument is that minimizing $\mathbf{W}^0\Theta\mathbf{d}$, and therefore optimize the accuracy of the subpopulation motif approach, is approximately achieved by minimizing $\|\Theta\mathbf{d}\|_2$. $\|\Theta\mathbf{d}\|_2$ is determined by the difference between \mathbf{d} and an approximation of \mathbf{d} using piecewise constant vectors associated with the subpopulations, which will be different when we choose different cut-offs ranks in the degree list. These arguments are confirmed by Fig. 8(a), where the cut-offs indicated by the analysis above reliably lie around the empirically observed optimal value (50) shown in Fig. 3(b) of the main text.

Extensions to more subpopulations: Following the arguments above, one can refine the division of subpopulations in the Barábasi-Albert network to further improve the accuracy of the cumulant approach. The Barábasi-Albert network can be viewed as a stochastic block model in the limit with large number of subpopulation. This can be confirmed by define a Θ that maps \mathbf{d} exactly to 0. Indeed, the corresponding cumulant approximations almost converge immediately at first order as in stochastic block models (SI Fig. 8(b), compare with Fig. 3(a) of the main text).



SI Fig. 8: (a) L_2 norm of the difference between the degree list (normalized) and the piecewise constant vector (see text) given by a certain cut-off. Different shades are 4 realizations of Barábasi-Albert networks (with same parameters). The legend is the cut-off value that achieves the minimum of difference. (b) Same as Fig. 5(b) for the 4 realizations of Barábasi-Albert networks, using $\Theta = \mathbf{I} - \mathbf{d}\mathbf{d}^T$ in Eq. (7) (dashed lines) for predicting the weighted average $\frac{1}{N}\mathbf{d}^T\mathbf{S}_y\mathbf{d}/S_x$. The solid lines are using the moment approach (Eq. (6) of the main text) with a similar replacement of $\langle\mathbf{A}\rangle$ by the weighted average $\frac{1}{N}\mathbf{d}^T\mathbf{A}\mathbf{d}$.

Subpopulation cumulant approach

Eq. (7) of the main text relates average correlations to motif cumulants for a single population. Through a similar derivation (see [Hu et al., 2012] for details), we arrive at an expression for average correlation in terms of multi-population motif cumulants:

$$\begin{aligned} \langle \mathbf{S}_y \rangle_B / S_x &:= \mathbf{D} \mathbf{U}^T \mathbf{S}_y \mathbf{U} \mathbf{D} / S_x \\ &= \frac{1}{N} \left(\mathbf{I} - \sum_{n=1}^{\infty} (N \tilde{A} w)^n \boldsymbol{\kappa}_n \mathbf{E} \right)^{-1} \left(\mathbf{E}^{-1} + \sum_{n,m=1}^{\infty} (N \tilde{A} w)^{n+m} \boldsymbol{\kappa}_{n,m} \right) \\ &\quad \cdot \left(\mathbf{I} - \sum_{m=1}^{\infty} (N \tilde{A} w)^m \mathbf{E} \boldsymbol{\kappa}_m \right)^{-1}. \end{aligned} \quad (15)$$

where $\mathbf{D} = \text{diag}\{1/\sqrt{N_1}, \dots, 1/\sqrt{N_b}\}$, $\mathbf{E} = \frac{1}{N} \mathbf{D}^{-2} = \text{diag}\{N_1/N, \dots, N_b/N\}$, the matrix \mathbf{U} is given by $\mathbf{U} = [\mathbf{u}_1 | \dots | \mathbf{u}_k]$, and $\mathbf{u}_i = (0, \dots, 0, 1, \dots, 1, 0 \dots, 0)^T / \sqrt{N_i}$ is the vector where the nonzero entries appear only at indices that match one of the nodes in the given subpopulation, normalized to unit L_2 norm. Here $\langle \mathbf{S}_y \rangle_B$ represents a block-wise average over entries corresponding to each subpopulation. We note that by taking the appropriate weighted average of these block-wise averages, we arrive again at Eq. (7) of the main text.

Similarly, we can express the third order coherence in terms of motif cumulants for networks with multiple subpopulations:

$$\begin{aligned} \langle \mathbf{S}_{y[3]} \rangle / S_{x[3]} &= \frac{1}{N^2} \left(\mathbf{I} - \sum_{l=1}^{\infty} (N \tilde{A} w)^l \boldsymbol{\kappa}_l \mathbf{E} \right)^{-1} \otimes \left(\mathbf{I} - \sum_{m=1}^{\infty} (N \tilde{A} w)^m \boldsymbol{\kappa}_m \mathbf{E} \right)^{-1} \otimes \left(\mathbf{I} - \sum_{n=1}^{\infty} (N \tilde{A} w)^n \boldsymbol{\kappa}_n \mathbf{E} \right)^{-1} \\ &\quad \cdot \left(\mathbf{E}_{[3]}^{-2} + \sum_{l,m=1}^{\infty} (N \tilde{A} w)^{l+m} (\boldsymbol{\kappa}_{l,m,\cdot} + \boldsymbol{\kappa}_{l,\cdot,m} + \boldsymbol{\kappa}_{\cdot,l,m}) + \sum_{l,m,n=1}^{\infty} (N \tilde{A} w)^{l+m+n} \boldsymbol{\kappa}_{l,m,n} \right). \end{aligned} \quad (16)$$

Here $\mathbf{E}_{[3]} = \text{diag}_{[3]}\{N_1/N, \dots, N_b/N\}$ is a diagonal tensor. The motif cumulant $\boldsymbol{\kappa}_{l,m,\cdot}$ is a tensor defined as

$$(\boldsymbol{\kappa}_{l,m,\cdot})^{\alpha\beta\gamma} = \frac{1}{N^{l+m-2}} (\mathbf{D} \mathbf{U}^T \mathbf{K}_l \boldsymbol{\Theta}_\gamma \mathbf{K}_m^T \mathbf{U} \mathbf{D})_{\alpha\beta} D_\gamma^2. \quad (17)$$

This corresponds to a two branch motif, with two endpoints in population α and β , and apex root in population γ . Similarly, $\boldsymbol{\kappa}_{l,\cdot,m}$ and $\boldsymbol{\kappa}_{\cdot,l,m}$ are simply transpositions of the tensor $\boldsymbol{\kappa}_{l,m,\cdot}$, i.e. $(\boldsymbol{\kappa}_{l,m,\cdot})^{\alpha\beta\gamma} = (\boldsymbol{\kappa}_{l,\cdot,m})^{\alpha\gamma\beta} = (\boldsymbol{\kappa}_{\cdot,l,m})^{\gamma\alpha\beta}$. Eq. (16) may be verified using Prop. 3, which is stated and proven below.

Note the block average of a $N \times N \times N$ tensor \mathbf{A} may be written as³ $\langle \mathbf{A} \rangle_B = (\mathbf{D} \mathbf{U}^T) \otimes (\mathbf{D} \mathbf{U}^T) \otimes (\mathbf{D} \mathbf{U}^T) \cdot \mathbf{A}$. Applying this averaging identity to Eq. (11) gives that

$$\langle \mathbf{S}_{y[3]} \rangle_B / S_{x[3]} = (\mathbf{D} \mathbf{U}^T) \otimes (\mathbf{D} \mathbf{U}^T) \otimes (\mathbf{D} \mathbf{U}^T) \cdot (\mathbf{P} \otimes \mathbf{P} \otimes \mathbf{P} \cdot \mathbf{I}_{[3]}) = (\mathbf{D} \mathbf{U}^T \mathbf{P}) \otimes (\mathbf{D} \mathbf{U}^T \mathbf{P}) \otimes (\mathbf{D} \mathbf{U}^T \mathbf{P}) \cdot \mathbf{I}_{[3]}.$$

This block average can again be further combined to get the overall average (Eq. (13) of the main text).

³Here $\mathbf{P} \otimes \mathbf{Q} \otimes \mathbf{R} \cdot \mathbf{A}$ is understood as the tensor product of matrices $\mathbf{P} \otimes \mathbf{Q} \otimes \mathbf{R}$ acting on a tensor \mathbf{A} , that is, $(\mathbf{P} \otimes \mathbf{Q} \otimes \mathbf{R} \cdot \mathbf{A})^{ijk} = \mathbf{P}_p^i \mathbf{Q}_q^j \mathbf{R}_r^k \mathbf{A}^{pqr}$.

Explicit expressions for motif cumulants

Motif cumulants for second order correlations, single population: Here, we will prove the following explicit expressions for κ_n and $\kappa_{n,m}$ which are equivalent to the recursive definition in Eqs. (8,9) of the main text:

$$\begin{aligned}\kappa_n &= \frac{1}{N^{n+1}} \sum_{i,j} \underbrace{(\mathbf{W}^0 \Theta \mathbf{W}^0 \dots \Theta \mathbf{W}^0)}_{n \text{ factors of } \mathbf{W}^0} ij \\ &= \frac{1}{N^n} \mathbf{u}^T [(\mathbf{W} \Theta)^{n-1} \mathbf{W}] \mathbf{u} \\ &= \frac{1}{N^n} \mathbf{u}^T \mathbf{W}_n^\theta \mathbf{u},\end{aligned}\tag{18}$$

$$\begin{aligned}\kappa_{n,m} &= \frac{1}{N^{n+m+1}} \sum_{i,j} \underbrace{(\mathbf{W}^0 \Theta \mathbf{W}^0 \dots \Theta \mathbf{W}^0)}_{n \text{ factors of } \mathbf{W}^0} \Theta \underbrace{\mathbf{W}^{0T} \Theta \mathbf{W}^{0T} \dots \Theta \mathbf{W}^{0T}}_{m \text{ factors of } \mathbf{W}^{0T}} ij \\ &= \frac{1}{N^{n+m}} \mathbf{u}^T [(\mathbf{W} \Theta)^{n-1} \mathbf{W} \Theta \mathbf{W}^T (\Theta \mathbf{W}^T)^{m-1}] \mathbf{u} \\ &= \frac{1}{N^{n+m}} \mathbf{u}^T \mathbf{W}_n^\theta \Theta \mathbf{W}_m^\theta \mathbf{u},\end{aligned}\tag{19}$$

where

$$\mathbf{W}_n^\theta = [\mathbf{W}^0 \Theta]^{n-1} \mathbf{W}^0$$

and $\mathbf{u} = (1, \dots, 1)^T / \sqrt{N}$, $\mathbf{H} = \mathbf{u} \mathbf{u}^T$, $\Theta = \mathbf{I} - \mathbf{H}$.

We will assume Eq. (18) is true and demonstrate the proof of Eq. (19). A nearly identical (simpler) proof verifies Eq. (18). First, recalling that $\mu_{n,m} = \langle \mathbf{W}^{0n} (\mathbf{W}^{0m})^T \rangle / N^{n+m-1}$, it is straightforward to verify that

$$\mu_{n,m} = \frac{1}{N^{n+m}} \mathbf{u}^T (\mathbf{W}^0)^n (\mathbf{W}^{0T})^m \mathbf{u}.\tag{20}$$

Substituting $\mathbf{I} = \Theta + \mathbf{H}$ between every subsequent appearance of the adjacency matrix \mathbf{W}^0 gives

$$\mu_{n,m} = \frac{1}{N^{n+m}} \mathbf{u}^T [\mathbf{W}^0 (\Theta + \mathbf{H})]^{n-1} \mathbf{W}^0 (\Theta + \mathbf{H}) \mathbf{W}^{0T} [(\Theta + \mathbf{H}) \mathbf{W}^{0T}]^{m-1} \mathbf{u}.\tag{21}$$

By expanding across all sums of $\Theta + \mathbf{H}$ except the central one (between the terms \mathbf{W}^0 , \mathbf{W}^{0T}), and noting that there is an obvious bijection between a pair of compositions of the integers n and m , *i.e.*, $\{n_1, \dots, n_t\} \in \mathcal{C}(n)$, $\{m_1, \dots, m_s\} \in \mathcal{C}(m)$, and a term of the form

$$\left[\prod_{i=1}^{t-1} (\mathbf{W}_{n_i}^\theta \mathbf{H}) \right] [\mathbf{W}_{n_t}^\theta (\Theta + \mathbf{H}) \mathbf{W}_{m_s}^\theta] \left[\prod_{j=1}^{s-1} (\mathbf{H} \mathbf{W}_{m_j}^\theta) \right]$$

we may write (using $\mathbf{H} = \mathbf{u}\mathbf{u}^T$)

$$\begin{aligned}
\boldsymbol{\mu}_{n,m} &= \frac{1}{N^{n+m}} \mathbf{u}^T \left\{ \sum_{\substack{\{n_1, \dots, n_t\} \in \mathcal{C}(n) \\ \{m_1, \dots, m_s\} \in \mathcal{C}(m)}}} \left[\prod_{i=1}^{t-1} (\mathbf{W}_{n_i}^\theta \mathbf{H}) \right] [\mathbf{W}_{n_t}^\theta (\boldsymbol{\Theta} + \mathbf{H}) \mathbf{W}_{m_s}^\theta \mathbf{u}] \left[\prod_{j=1}^{s-1} (\mathbf{H} \mathbf{W}_{m_j}^\theta) \right] \right\} \mathbf{u} \\
&= \frac{1}{N^{n+m}} \sum_{\substack{\{n_1, \dots, n_t\} \in \mathcal{C}(n) \\ \{m_1, \dots, m_s\} \in \mathcal{C}(m)}}} \left[\prod_{i=1}^{t-1} (\mathbf{u}^T \mathbf{W}_{n_i}^\theta \mathbf{u}) \right] [\mathbf{u}^T \mathbf{W}_{n_t}^\theta (\boldsymbol{\Theta} + \mathbf{u}\mathbf{u}^T) \mathbf{W}_{m_s}^\theta \mathbf{u}] \left[\prod_{j=1}^{s-1} (\mathbf{u}^T \mathbf{W}_{m_j}^\theta \mathbf{u}) \right] \\
&= \sum_{\substack{\{n_1, \dots, n_t\} \in \mathcal{C}(n) \\ \{m_1, \dots, m_s\} \in \mathcal{C}(m)}}} \left[\prod_{i=1}^{t-1} \left(\frac{1}{N^{n_i}} \mathbf{u}^T \mathbf{W}_{n_i}^\theta \mathbf{u} \right) \right] \left[\frac{1}{N^{n_t+m_s}} \mathbf{u}^T \mathbf{W}_{n_t}^\theta (\boldsymbol{\Theta} + \mathbf{u}\mathbf{u}^T) \mathbf{W}_{m_s}^\theta \mathbf{u} \right] \\
&\quad \cdot \left[\prod_{j=1}^{s-1} \left(\frac{1}{N^{m_j}} \mathbf{u}^T \mathbf{W}_{m_j}^\theta \mathbf{u} \right) \right]
\end{aligned} \tag{22}$$

If $t = 1$, we define the product $\left[\prod_{i=1}^{t-1} (\mathbf{W}_{n_i}^\theta \mathbf{H}) \right] = \mathbf{I}$.

We now prove Eq. (19) by induction, assuming Eq. (18) holds. First, when $n = m = 1$, the only compositions are trivial (i.e., $\pi_1 = \pi_2 = \{1\}$). Equating in this case the right-hand sides of Eq. (9) of the main text and Eq. (22) gives that

$$\boldsymbol{\kappa}_{1,1} + (\boldsymbol{\kappa}_1)^2 = \frac{1}{N^2} \mathbf{u}^T \mathbf{W}_1^\theta \boldsymbol{\Theta} \mathbf{W}_1^\theta \mathbf{u} + \left(\frac{1}{N} \mathbf{u}^T \mathbf{W}_1^\theta \mathbf{u} \right)^2$$

Since Eq. (18) for $n = 1$ gives that

$$\boldsymbol{\kappa}_1 = \frac{1}{N} \mathbf{u}^T \mathbf{W}_1^\theta \mathbf{u},$$

we have that Eq. (19) holds for $n = m = 1$. Next, assume Eq. (19) is true for all (p, q) such that $p \leq n$ and $q < m$ or $p < n$ and $q \leq m$. That is, in these cases,

$$\boldsymbol{\kappa}_p = \frac{1}{N^p} \mathbf{u}^T \mathbf{W}_p^\theta \mathbf{u} \text{ (by Eq. (18))} \quad \text{and} \quad \boldsymbol{\kappa}_{p,q} = \frac{1}{N^{p+q}} \mathbf{u}^T \mathbf{W}_p^\theta \boldsymbol{\Theta} \mathbf{W}_q^\theta \mathbf{u}.$$

Making the corresponding substitutions in Eq. (22), the only term we have not accounted for in matching the right-hand side of Eq. (22) to that of Eq. (9) of the main text are the terms corresponding to the pair of compositions $\{n\}, \{m\}$. In Eq. (9) of the main text, the corresponding terms are

$$\boldsymbol{\kappa}_{n,m} + \boldsymbol{\kappa}_n \boldsymbol{\kappa}_m \tag{23}$$

while in Eq. (22), the terms take the form

$$\begin{aligned}
\frac{1}{N^{n+m}} \mathbf{u}^T \mathbf{W}_n^\theta (\boldsymbol{\Theta} + \mathbf{u}\mathbf{u}^T) \mathbf{W}_m^\theta \mathbf{u} &= \frac{1}{N^{n+m}} \mathbf{u}^T \mathbf{W}_n^\theta \boldsymbol{\Theta} \mathbf{W}_m^\theta \mathbf{u} + \left(\frac{1}{N^n} \mathbf{u}^T \mathbf{W}_n^\theta \mathbf{u} \right) \left(\frac{1}{N^m} \mathbf{u}^T \mathbf{W}_m^\theta \mathbf{u} \right) \\
&= \frac{1}{N^{n+m}} \mathbf{u}^T \mathbf{W}_n^\theta \boldsymbol{\Theta} \mathbf{W}_m^\theta \mathbf{u} + \boldsymbol{\kappa}_n \boldsymbol{\kappa}_m,
\end{aligned} \tag{24}$$

where the second equality follows from the inductive assumption. Equating Eqns. (23,24) gives that

$$\boldsymbol{\kappa}_{n,m} = \frac{1}{N^{n+m}} \mathbf{u}^T \mathbf{W}_n^\theta \boldsymbol{\Theta} \mathbf{W}_m^\theta \mathbf{u},$$

which is exactly Eq. (19), completing the inductive proof.

Motif cumulants for second order correlations, multiple subpopulations: Eq. (15) gives a representation of average correlation in terms of motif cumulants under the assumption of multiple subpopulations. The recursive decomposition relationships for subpopulation motif moments and cumulants are

$$\boldsymbol{\mu}_n = \sum_{\{n_1, \dots, n_t\} \in \mathcal{C}(n)} \left[\left(\prod_{i=1}^{t-1} \boldsymbol{\kappa}_{n_i} \mathbf{E} \right) \boldsymbol{\kappa}_{n_t} \right] \quad (25)$$

$$\boldsymbol{\mu}_{n,m} = \sum_{\substack{\{n_1, \dots, n_t\} \in \mathcal{C}(n) \\ \{m_1, \dots, m_s\} \in \mathcal{C}(m)}} \left(\prod_{i=1}^{t-1} \boldsymbol{\kappa}_{n_i} \mathbf{E} \right) (\boldsymbol{\kappa}_{n_t, m_s} + \boldsymbol{\kappa}_{n_t} \mathbf{E} \boldsymbol{\kappa}_{m_s}) \left(\prod_{j=1}^{s-1} \mathbf{E} \boldsymbol{\kappa}_{m_j} \right). \quad (26)$$

Here $\mathbf{E} = \text{diag}\{N_1/N, \dots, N_b/N\}$ (b is the number of subpopulations, having sizes N_i , where $\sum N_i = N$) is inserted between each motif cumulant matrix multiplication and yields the appropriate weighted sums for the interpretation of the terms $\boldsymbol{\mu}_{n,m}$ and $\boldsymbol{\kappa}_{n,m}$ as *probabilities* (specifically, scaling by \mathbf{E} is multiplication by the probability of selecting cells from respective populations at “breaks” in the motifs). Moreover we have an explicit expression for motif cumulants similar to Eq. (19):

$$\boldsymbol{\kappa}_{n,m} = \frac{1}{N^{n+m-1}} \mathbf{D} \mathbf{U}^T \underbrace{\mathbf{W}^0 \boldsymbol{\Theta} \mathbf{W}^0 \dots \boldsymbol{\Theta} \mathbf{W}^0}_{n \text{ factors of } \mathbf{W}^0} \boldsymbol{\Theta} \underbrace{\mathbf{W}^{0T} \boldsymbol{\Theta} \mathbf{W}^{0T} \dots \boldsymbol{\Theta} \mathbf{W}^{0T}}_{m \text{ factors of } \mathbf{W}^{0T}} \mathbf{U} \mathbf{D}, \quad (27)$$

where, again, $\mathbf{D} = \text{diag}\{1/\sqrt{N_1}, \dots, 1/\sqrt{N_b}\}$, $\boldsymbol{\Theta} = \mathbf{I} - \mathbf{H}$, $\mathbf{H} = \mathbf{U} \mathbf{U}^T$, the matrix \mathbf{U} is given by $\mathbf{U} = [\mathbf{u}_1 | \dots | \mathbf{u}_k]$, and $\mathbf{u}_i = (0, \dots, 0, 1, \dots, 1, 0 \dots, 0)^T / \sqrt{N_i}$ is the vector where the nonzero entries appear only at indices that match one of the nodes in the given subpopulation, normalized to unit L_2 norm. This formula can be proved identically to Eq. (19) by considering the relationship between $\frac{1}{N} \mathbf{D}^{-1} \boldsymbol{\mu}_{n,m} \mathbf{D}^{-1}$ and $\frac{1}{N} \mathbf{D}^{-1} \boldsymbol{\kappa}_{n,m} \mathbf{D}^{-1}$ and noting that $\mathbf{E} = \frac{1}{N} \mathbf{D}^{-2}$.

Motif cumulants for third order correlations: The explicit expressions of motif cumulants in Eqns. (19, 27) also generalize to higher orders. For example, for third-order motif cumulants,

$$\boldsymbol{\kappa}_{l,m,n} = \frac{1}{N^{l+m+n+1}} \sum_{i,j,k} (\mathbf{W}_n^\theta)_p^i (\mathbf{W}_m^\theta)_q^j (\mathbf{W}_l^\theta)_r^k \boldsymbol{\Phi}^{pqr}. \quad (28)$$

The tensor $\boldsymbol{\Phi}$ is defined in Prop. 1.

For the third order multipopulation case

$$\kappa_{l,m,n} = \frac{1}{N^{l+m+n-2}} (\mathbf{D}\mathbf{U}^T \mathbf{W}_l^\theta) \otimes (\mathbf{D}\mathbf{U}^T \mathbf{W}_m^\theta) \otimes (\mathbf{D}\mathbf{U}^T \mathbf{W}_n^\theta) \cdot \Phi. \quad (29)$$

Here Φ is the block diagonal tensor defined in Prop. 3. The summation of α is over all subpopulations, and the block tensor Φ_α is defined in Prop. 3.

Proof of the third order cumulant approach Eq. (13) (main text)

In Eq. (13) of the main text, we expressed average third-order correlation in terms of motif cumulants. Here, we provide the proof of this relationship. We will first prove a proposition and Eq. (13) follows directly.

Proposition 1. *Let \mathbf{H} be the rank-1 orthogonal projection matrix generated by the unit N -vector $\mathbf{u} = (1, \dots, 1)/\sqrt{N}$, $\mathbf{H} = \mathbf{u}\mathbf{u}^T$, $\Theta = \mathbf{I} - \mathbf{H}$, tensor $\Phi^{ijk} = \delta^{ijk} - \Theta^{ij}u^k/\sqrt{N} - \Theta^{ik}u^j/\sqrt{N} - \Theta^{jk}u^i/\sqrt{N} - u^i u^j u^k/\sqrt{N}$. δ^{pqr} is the Kronecker delta. We use Einstein summation convention and $\mathbf{P}_j^i = \mathbf{P}_{ij} = \mathbf{P}^{ij}$, $u^i = u_i$. For any $N \times N$ matrix \mathbf{K} , let*

$$\mathbf{K}_n = (\mathbf{K}\Theta)^{n-1} \mathbf{K} = \underbrace{\mathbf{K}\Theta\mathbf{K}\dots\Theta\mathbf{K}}_{n \text{ factors of } \mathbf{K}}, \quad \mathbf{P} = (\mathbf{I} - \mathbf{K})^{-1}$$

If the spectral radii $\Psi(\mathbf{K}) < 1$ and $\Psi(\mathbf{K}\Theta) < 1$, then

$$\begin{aligned} & \sqrt{N}u_i u_j u_k \mathbf{P}_p^i \mathbf{P}_q^j \mathbf{P}_r^k \delta^{pqr} \\ &= \left(1 - \sum_{l=1}^{\infty} \mathbf{u}^T \mathbf{K}_l \mathbf{u}\right)^{-1} \left(1 - \sum_{m=1}^{\infty} \mathbf{u}^T \mathbf{K}_m \mathbf{u}\right)^{-1} \left(1 - \sum_{n=1}^{\infty} \mathbf{u}^T \mathbf{K}_n \mathbf{u}\right)^{-1} \\ & \cdot \left(1 + 3 \sum_{l,m=1}^{\infty} \mathbf{u}^T \mathbf{K}_l \Theta \mathbf{K}_m^T \mathbf{u} + \sqrt{N} \sum_{l,m,n=1}^{\infty} u_i u_j u_k (\mathbf{K}_l)_p^i (\mathbf{K}_m)_q^j (\mathbf{K}_n)_r^k \Phi^{pqr}\right). \end{aligned} \quad (30)$$

Proof. Note that,

$$\begin{aligned} & \sqrt{N}u_i u_j u_k \mathbf{P}_p^i \mathbf{P}_q^j \mathbf{P}_r^k \delta^{pqr} \\ &= \sqrt{N}u_i u_j u_k \mathbf{P}_p^i \mathbf{P}_q^j \mathbf{P}_r^k (u^p u^q u^r / \sqrt{N} + \Theta^{pq} u^r / \sqrt{N} + \Theta^{pr} u^q / \sqrt{N} + \Theta^{qr} u^p / \sqrt{N} + \Phi^{pqr}) \\ &= (u_i \mathbf{P}_p^i u^p)(u_j \mathbf{P}_q^j u^q)(u_k \mathbf{P}_r^k u^r) + 3(u_i \mathbf{P}_p^i \Theta^{pq} \mathbf{P}_q^j u_j)(u_k \mathbf{P}_r^k u^r) \\ & \quad + \sqrt{N}u_i u_j u_k \mathbf{P}_p^i \mathbf{P}_q^j \mathbf{P}_r^k \Phi^{pqr} \\ &= (\mathbf{u}^T \mathbf{P} \mathbf{u})^3 + 3(\mathbf{u}^T \mathbf{P} \mathbf{u})(\mathbf{u}^T \mathbf{P} \Theta \mathbf{P}^T \mathbf{u}) + \sqrt{N}u_i u_j u_k \mathbf{P}_p^i \mathbf{P}_q^j \mathbf{P}_r^k \Phi^{pqr}. \end{aligned} \quad (31)$$

Using Prop. 4.1 in [Hu et al., 2012] gives alternate forms for the first two terms on the right hand side of Eq. (31):

$$\begin{aligned} \mathbf{u}^T \mathbf{P} \mathbf{u} &= \left(1 - \sum_{l=1}^{\infty} \mathbf{u}^T \mathbf{K}_l \mathbf{u}\right)^{-1} \\ \mathbf{u}^T \mathbf{P} \Theta \mathbf{P}^T \mathbf{u} &= \left(1 - \sum_{l=1}^{\infty} \mathbf{u}^T \mathbf{K}_l \mathbf{u}\right)^{-2} \left(\sum_{l,m=1}^{\infty} \mathbf{u}^T \mathbf{K}_l \Theta \mathbf{K}_m^T \mathbf{u}\right) \end{aligned} \quad (32)$$

To rewrite the third term, we use a combinatorial lemma similar to that in [Hu et al., 2012].

Lemma 2. *Let $\{x_l\}_{l \geq 1}$, $\{y_m\}_{m \geq 1}$, $\{z_n\}_{n \geq 1}$, $\{w_{lmn}\}_{l,m,n \geq 1}$ be sequences which converge absolutely when summed, and also satisfy*

$$\left| \sum_{l=1}^{\infty} x_l \right| < 1, \quad \left| \sum_{m=1}^{\infty} y_m \right| < 1, \quad \left| \sum_{n=1}^{\infty} z_n \right| < 1.$$

Then,

$$\begin{aligned} & \sum_{i,j,k=1}^{\infty} \sum_{\substack{\{l_1, \dots, l_{p+1}\} \in \mathcal{C}(i) \\ \{m_1, \dots, m_{q+1}\} \in \mathcal{C}(j) \\ \{n_1, \dots, n_{r+1}\} \in \mathcal{C}(k)}} \left[\left(\prod_{s=1}^p x_{l_s} \right) \left(\prod_{t=1}^q y_{m_t} \right) \left(\prod_{u=1}^r z_{n_u} \right) w_{l_{p+1} m_{q+1} n_{r+1}} \right] \\ &= \left[\sum_{i=0}^{\infty} \left(\sum_{l=1}^{\infty} x_l \right)^i \right] \left[\sum_{j=0}^{\infty} \left(\sum_{m=1}^{\infty} y_m \right)^j \right] \left[\sum_{k=0}^{\infty} \left(\sum_{n=1}^{\infty} z_n \right)^k \right] \left(\sum_{l,n,m=1}^{\infty} w_{lmn} \right). \end{aligned}$$

where the sum over $\{n_1, \dots, n_{r+1}\} \in \mathcal{C}(k)$ is as defined in the proof of Eqs. (18,19).

Similar to proofs for second order covariances given in [Hu et al., 2012], using Lemma 2 and expanding \mathbf{P} as a power series in \mathbf{K} , we can show that the third term in Eq. (31) may be rewritten

$$u_i u_j u_k \mathbf{P}_p^i \mathbf{P}_q^j \mathbf{P}_r^k \Phi^{pqr} = \left(1 - \sum_{n=1}^{\infty} \mathbf{u}^T \mathbf{K}_n \mathbf{u} \right)^{-3} \left(\sum_{l,m,n=1}^{\infty} u_i u_j u_k (\mathbf{K}_l)_p^i (\mathbf{K}_m)_q^j (\mathbf{K}_n)_r^k \Phi^{pqr} \right). \quad (33)$$

Substituting Eqs. (32,33) in to Eq. (31) gives Eq. (30) after an analytical continuation argument similar to that used for the second order analog of Eq. (13) of the main text, as shown in [Hu et al., 2012]. □

Finally, to get Eq. (13) of the main text, let $\mathbf{K} = \tilde{A} w \mathbf{W}^0$ in Prop. 1, note that $N^{-\frac{3}{2}} u_i u_j u_k \mathbf{S}_{y[3]}^{ijk} = \langle \mathbf{S}_{y[3]} \rangle$, and use the explicit formulas of motif cumulants Eq. (18),(19) and (28).

Proof of the third order subpopulation cumulant approach SI Eq. (16)

The subpopulation cumulant approach for third order correlation is backed up by the following proposition.

Proposition 3. *Let $\mathbf{U} = (\mathbf{u}_1 | \dots | \mathbf{u}_b)$, and $\mathbf{u}_i = (0, \dots, 0, 1, \dots, 1, 0 \dots, 0)^T / \sqrt{N_i}$ be the L^2 unit vector having entries of zero outside of positions corresponding to population i . Also, define the 3-dimensional diagonal tensor*

$$\mathbf{D}_{[3]} = \text{diag}_{[3]} \{1/\sqrt{N_1}, \dots, 1/\sqrt{N_b}\},$$

$\mathbf{H} = \mathbf{U}\mathbf{U}^T$, and $\mathbf{\Theta} = \mathbf{I} - \mathbf{H}$. We refer to the diagonal elements of $\mathbf{D}_{[3]}$ as D_α . The tensor $\mathbf{\Phi}$ is given by

$$(\mathbf{\Phi})^{ijk} = \delta^{ijk} - \sum_{\alpha=1}^b (\mathbf{\Theta}_\alpha^{ij} u_\alpha^k D_\alpha - \mathbf{\Theta}_\alpha^{ik} u_\alpha^j D_\alpha - \mathbf{\Theta}_\alpha^{jk} u_\alpha^i D_\alpha - u_\alpha^i u_\alpha^j u_\alpha^k D_\alpha).$$

where δ^{ijk} is the Kronecker delta, and $(\mathbf{I}_{[3]})^{ijk} = \delta^{ijk}$. Here $(\mathbf{\Theta}_\alpha)^{ij} := \mathbf{\Theta}_\alpha^{ij} = \mathbf{\Theta}^{ij}$ if i, j are both indices in population α or 0 otherwise, is the block of $\mathbf{\Theta}$ corresponding to population α and $\mathbf{\Theta} = \sum_\alpha \mathbf{\Theta}_\alpha$. Note that $\mathbf{\Phi}$ has a block diagonal structure $\mathbf{\Phi} = \sum_\alpha \mathbf{\Phi}_\alpha$, where $\mathbf{\Phi}_\alpha$ is defined as the block of $\mathbf{\Phi}$: $(\mathbf{\Phi}_\alpha)^{ijk} = \mathbf{\Phi}^{ijk}$ if i, j, k are all indices in population α or 0 otherwise. Over each block, $\mathbf{\Phi}_\alpha$ has a similar expressions as $\mathbf{\Phi}$ in Prop. 1. We use Einstein summation convention and $\mathbf{A}_j^i = \mathbf{A}_{ij} = \mathbf{A}^{ij}$, $u^i = u_i$. For any $N \times N$ matrix \mathbf{K} , let

$$\mathbf{K}_n = (\mathbf{K}\mathbf{\Theta})^{n-1} \mathbf{K} = \underbrace{\mathbf{K}\mathbf{\Theta}\mathbf{K} \cdots \mathbf{\Theta}\mathbf{K}}_{n \text{ factors of } \mathbf{K}}, \quad \mathbf{P} = (\mathbf{I} - \mathbf{K})^{-1}$$

If the spectral radii $\Psi(\mathbf{K}) < 1$ and $\Psi(\mathbf{K}\mathbf{\Theta}) < 1$, then

$$\begin{aligned} & (\mathbf{U}^T \mathbf{P}) \otimes (\mathbf{U}^T \mathbf{P}) \otimes (\mathbf{U}^T \mathbf{P}) \cdot \mathbf{I}_{[3]} \\ &= \left(\mathbf{I} - \sum_{l=1}^{\infty} \mathbf{U}^T \mathbf{K}_l \mathbf{U} \right)^{-1} \otimes \left(\mathbf{I} - \sum_{m=1}^{\infty} \mathbf{U}^T \mathbf{K}_m \mathbf{U} \right)^{-1} \otimes \left(\mathbf{I} - \sum_{n=1}^{\infty} \mathbf{U}^T \mathbf{K}_n \mathbf{U} \right)^{-1} \\ & \cdot \left(\mathbf{D}_{[3]} + \sum_{l,m=1}^{\infty} \mathbf{R}_{l,m} + \sum_{l,m,n=1}^{\infty} (\mathbf{U}^T \mathbf{K}_l) \otimes (\mathbf{U}^T \mathbf{K}_m) \otimes (\mathbf{U}^T \mathbf{K}_n) \cdot \mathbf{\Phi} \right), \end{aligned} \quad (34)$$

where

$$(\mathbf{R}_{l,m})^{\alpha\beta\gamma} = (\mathbf{U}^T \mathbf{K}_l \mathbf{\Theta}_\gamma \mathbf{K}_m^T \mathbf{U})_{\alpha\beta} D_\gamma + (\mathbf{U}^T \mathbf{K}_l \mathbf{\Theta}_\beta \mathbf{K}_m^T \mathbf{U})_{\alpha\gamma} D_\beta + (\mathbf{U}^T \mathbf{K}_l \mathbf{\Theta}_\alpha \mathbf{K}_m^T \mathbf{U})_{\beta\gamma} D_\alpha. \quad (35)$$

Proof. The proof parallels exactly the single population case Prop. 1. Using the definition of $\mathbf{\Phi}$, we have

$$\begin{aligned} & (\mathbf{U}^T \mathbf{P}) \otimes (\mathbf{U}^T \mathbf{P}) \otimes (\mathbf{U}^T \mathbf{P}) \cdot \mathbf{I}_{[3]} \\ &= (\mathbf{U}^T \mathbf{P} \mathbf{U}) \otimes (\mathbf{U}^T \mathbf{P} \mathbf{U}) \otimes (\mathbf{U}^T \mathbf{P} \mathbf{U}) \cdot \mathbf{D}_{[3]} + \mathbf{Q} \\ & \quad + (\mathbf{U}^T \mathbf{P}) \otimes (\mathbf{U}^T \mathbf{P}) \otimes (\mathbf{U}^T \mathbf{P}) \cdot \mathbf{\Phi}. \end{aligned} \quad (36)$$

where the tensor \mathbf{Q} is given by

$$\begin{aligned} \mathbf{Q}^{\alpha\beta\gamma} &= \sum_{\lambda} (\mathbf{U}^T \mathbf{P} \mathbf{\Theta}_\lambda \mathbf{P}^T \mathbf{U})^{\alpha\beta} (\mathbf{U}^T \mathbf{P} \mathbf{U})^\gamma D_\lambda + (\mathbf{U}^T \mathbf{P} \mathbf{\Theta}_\lambda \mathbf{P}^T \mathbf{U})^{\alpha\gamma} (\mathbf{U}^T \mathbf{P} \mathbf{U})^\beta D_\lambda \\ & \quad + (\mathbf{U}^T \mathbf{P} \mathbf{\Theta}_\lambda \mathbf{P}^T \mathbf{U})^{\beta\gamma} (\mathbf{U}^T \mathbf{P} \mathbf{U})^\alpha D_\lambda. \end{aligned} \quad (37)$$

Again, the third term is a new type not presented in second order correlation theory. It turns out that Lemma 2 holds for this multi-population case where the terms involved

are now matrices as opposed to scalars, and scalar multiplications become tensor products. Applying the lemma gives, via standard rules for tensor multiplication,

$$\begin{aligned} & (\mathbf{U}^T \mathbf{P}) \otimes (\mathbf{U}^T \mathbf{P}) \otimes (\mathbf{U}^T \mathbf{P}) \cdot \Phi \\ = & \left(\mathbf{I} - \sum_{l=1}^{\infty} \mathbf{U}^T \mathbf{K}_l \mathbf{U} \right)^{-1} \otimes \left(\mathbf{I} - \sum_{m=1}^{\infty} \mathbf{U}^T \mathbf{K}_m \mathbf{U} \right)^{-1} \otimes \left(\mathbf{I} - \sum_{n=1}^{\infty} \mathbf{U}^T \mathbf{K}_n \mathbf{U} \right)^{-1} \\ & \cdot \left(\sum_{l,m,n=1}^{\infty} (\mathbf{U}^T \mathbf{K}_l) \otimes (\mathbf{U}^T \mathbf{K}_m) \otimes (\mathbf{U}^T \mathbf{K}_n) \cdot \Phi \right). \end{aligned}$$

The rest of the proof is identical to the single population case. \square

Approximating the average correlation coefficient

The average covariance across the network, $\langle \mathbf{C}_y \rangle$ can be used to approximate the average correlation coefficient $\rho^{\text{avg}} = \sum_{i,j} \rho_{ij} / N^2$, $\rho_{ij} = \mathbf{C}_y^{ij} / \sqrt{\mathbf{C}_y^{ii} \mathbf{C}_y^{jj}}$. Here we describe two such approximations. First, when the uncoupled units have equal mean activities, and the perturbation from recurrent coupling is weak, the diagonal terms \mathbf{C}_y^{ii} will be close to the uncoupled values, C_x . In this case, subtracting diagonal terms from the average, we have that

$$\rho^{\text{avg}} \approx \left(\frac{\langle \mathbf{C}_y \rangle}{C_x} - \frac{1}{N} \right) \cdot \frac{N}{N-1}. \quad (38)$$

In a second, more accurate approximation, we assume permutation symmetry between nodes (within a population). Also, in our networks, self-connections are allowed and occur with the same probability as other connections. These will lead to identical (marginal) distributions for each entry in the covariance matrix \mathbf{C}_y , excepting the diagonal entries which are shifted by a constant of C_x due to each unit's own uncoupled variance (this corresponds to the term proportional to \mathbf{I} in expansion Eq. (5)). This suggests that \mathbf{C}_y has the form

$$\mathbf{C}_y \approx C_x \mathbf{I} + c \mathbf{1}_{NN},$$

where $\mathbf{1}_{NN}$ is the $N \times N$ matrix of ones, and c is a constant. Using the diagonal entries of this matrix to normalize, we obtain

$$\rho^{\text{avg}} \approx \frac{\langle \mathbf{C}_y \rangle - C_x / N}{C_x + \langle \mathbf{C}_y \rangle - C_x / N}. \quad (39)$$

These approximations can also be generalized to networks consisting of multiple sub-populations. For example a network with population A and B , we have analogs of Eqns. (38,39) for each of the average covariance within and between two populations A and B ,

$$\begin{aligned} \rho_{AA}^{\text{avg}} & \approx \left(\frac{\langle \mathbf{C}_y \rangle_{AA}}{C_x} - \frac{1}{N_A} \right) \cdot \frac{N_A}{N_A - 1}, \\ \rho_{AB}^{\text{avg}} & \approx \langle \mathbf{C}_y \rangle_{AB} / C_x, \end{aligned} \quad (40)$$

and

$$\begin{aligned}\rho_{AA}^{\text{avg}} &\approx \frac{\langle \mathbf{C}_y \rangle_{AA} - C_x/N_A}{C_x + \langle \mathbf{C}_y \rangle_{AA} - C_x/N_A}, \\ \rho_{AB}^{\text{avg}} &\approx \frac{\langle \mathbf{C}_y \rangle_{AB}}{\sqrt{(C_x + \langle \mathbf{C}_y \rangle_{AA} - C_x/N_A)(C_x + \langle \mathbf{C}_y \rangle_{BB} - C_x/N_B)}}.\end{aligned}\tag{41}$$